2025 IEEE Applied Power Electronics Conference and Exposition (APEC) | 979-8-3315-1611-6/25/$31.00 ©2025 IEEE | DOI: 10.1109/APEC48143.2025.10977109

Wireless Actuation of Magnetic Robots with a Modular 60 mT 3-D Helmholtz Coil System

Konstantinos Manos, Yifan Rao, Tuo Zhao, Kevin Liu, Daniel Zhou, Calvin Nguyen, Eric Chen, Glaucio H. Paulino, and Minjie Chen
Princeton University, Princeton, NJ, United States
Email: {km4382, minjie}@princeton.edu

***Abstract*—This paper presents the modeling and design of a three-dimensional (3-D) Helmholtz coil system for wireless control of magnetically actuated robots. Instead of using moving permanent magnets to generate the external magnetic field needed for magnetic actuation, driving a set of stationary Helmholtz coils with power electronics offers enhanced control flexibility and precision through active feedback. A modular drive is developed to operate the custom pulsed 15 kW 60 mT 3-D Helmholtz coil setup. A method for modeling the generated magnetic field is developed to enable the precise motion control of untethered robots. The prototype system is verified by precisely actuating a magnetized cubic robot.**

***Index Terms*—3-D Helmholtz coil system, modular drive, wireless actuation, magnetically actuated robot**

I. Introduction

THE inclusion of magnetic dipole elements in a robotic structure enables its remote manipulation under external magnetic fields. The dipoles tend to align with the applied field, generating torques, while magnetic field gradients produce forces that induce translational motion. When a dipole of magnetic moment $\mathbf{m}$ is subjected to an externally imposed flux density $\mathbf{b}$, the torque and the translational force exerted on the dipole are given [1] by

$$\boldsymbol{\tau} = \mathbf{m} \times \mathbf{b}, \tag{1}$$

$$\mathbf{f} = (\mathbf{m} \cdot \nabla)\mathbf{b}. \tag{2}$$

By leveraging the aforementioned interaction between the dipole elements embedded in the robot and the external magnetic field, sophisticated robotic motion patterns can be realized.

Owing to their simplicity – stemming from the absence of complex moving parts, external wires, and an onboard energy source – magnetically actuated robots are well-suited for critical, confined-space applications such as biomedical settings and harsh environments. These robots can take various forms, ranging from digestible capsules [2]–[4] to sophisticated robotic arms [5], [6]. While some works have relied on moving permanent magnets for generating the required external magnetic field [2], [5], this approach entails limited control speed and modulation capability and it increases the system complexity requiring an additional robot to move the permanent magnet.

In this paper we focus on using a set of stationary current-carrying coils for generating the required magnetic field. A modular drive system is designed for controlling the coil currents to the desired values resulting in the precise actuation of a magnetically actuated robot. A complete wireless actuation setup is presented in Fig. 1. Such a system enables fully untethered operation of the magnetic robots. Rapid and precise control of the magnetic field enables the robot to perform sophisticated tasks with high agility and a large number of control degrees of freedom.

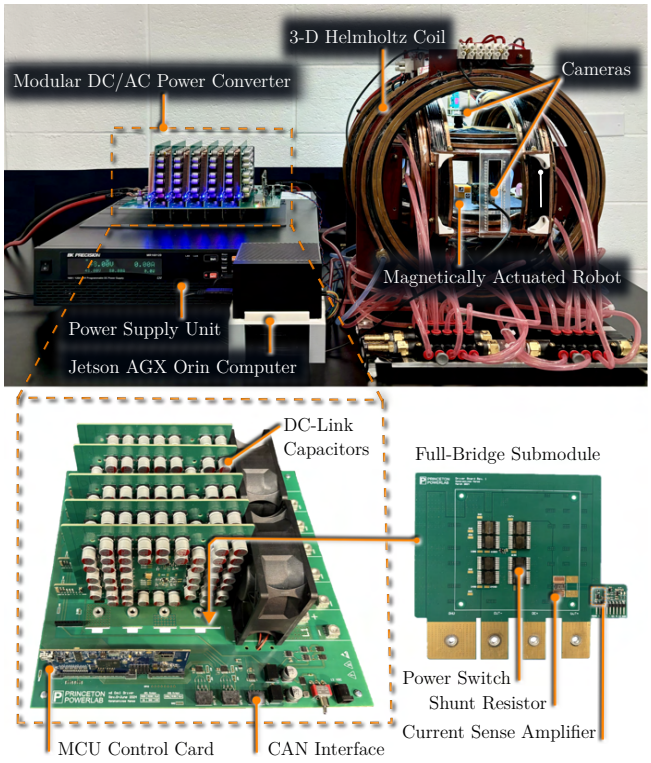
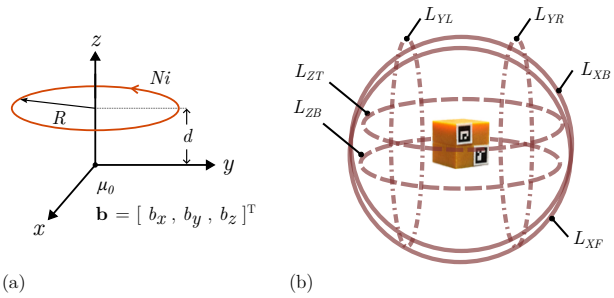


Fig. 1. Wireless magnetic robotic actuation system comprising a dc power source, a scalable power converter, and a set of copper coils. Cameras are mounted around the coil to monitor the robot motion. The video data is analyzed in real time on an NVIDIA Jetson AGX Orin computer.

This paper is organized as follows: Section II introduces the 3-D Helmholtz coil structure and presents an analytical model enabling the mapping between the flux density and the coil currents in 3-D space and the sizing of the coil system. It then elaborates on the design of a modular dc-ac power

Authorized licensed use limited to: Princeton University. Downloaded on November 14,2026 at 21:21:41 UTC from IEEE Xplore. Restrictions apply.



(a) (b)

Fig. 2. (a) A filamentary circular loop of radius R carrying a current Ni placed at an offset d from the xy plane is used to model each winding of the coil system; (b) 3-D Helmholtz coil structure made of 6 individual circular windings. The first subscript indicates the axial direction, while the second denotes the relative position.: left/right (L/R), front/back (F/B), and top/bottom (T/B). Same-axis windings are identical.

converter used for the precise control of the individual winding currents. Section III presents experimental results highlighting the field generation capabilities of the setup and demonstrates the locomotion of a cubic robot as an example of magnetic robot actuation. Finally, Section IV concludes this paper.

II. System Modeling and Design

To precisely control a magnetically actuated robot, the mapping between the coil currents and the magnetic field at the robot location needs to be determined first. The individual winding currents are then independently controlled by a drive system maintaining the desired reference values irrespective of the operating conditions.

A. 3-D Helmholtz Coil System

The fundamental building block of the coil system is a circular current-carrying winding. We model an N-turn winding by an equivalent filamentary circular loop of radius R corresponding to the mean radius of the winding carrying a current Ni, as shown in Fig. 2-(a). To maximize the robot actuation freedom, the magnetic field needs to be controlled in all 3 dimensions. A pair of coaxial loops, known as a Helmholtz coil system, can generate either an approximately uniform or a high-gradient field along the axial direction when the current directions are equal or opposite respectively. Arranging 3 such pairs perpendicular to each other, as illustrated in Fig. 2-(b), results in a coil system that allows control of the field in any direction. Due to symmetry, the windings of a coaxial pair should be identical and placed equally away from the origin. However, the windings of different axes need not have the same radii, number turns, and offset from the origin. In fact, it is convenient that their geometrical characteristics are different so that a compact 3-D coil system can be formed.

The flux density $\mathbf{b}(x,y,z)$ at any point $P(x,y,z)$ in a 3-D space produced by the circular loop of Fig. 2-(a) can be expressed [7] as

$$b_x = \frac{C\cdot x\cdot(z-d)}{2\cdot A^2\cdot B\cdot \rho^2}\cdot\left[(R^2+r^2)\cdot E(k^2)-A^2\cdot K(k^2)\right], \tag{3}$$

$$b_z = \frac{C}{2\cdot A^2\cdot B}\cdot\left[(R^2-r^2)\cdot E(k^2)+A^2\cdot K(k^2)\right], \tag{4}$$

$$b_y = \frac{y}{x}\cdot b_x, \tag{5}$$

where R is the radius of the loop and

$$\begin{aligned}
\rho &= \sqrt{x^2+y^2},\\
r^2 &= x^2+y^2+(z-d)^2,\\
k^2 &= 1-\frac{A^2}{B^2},\\
A^2 &= R^2+r^2-2R\rho,\\
B^2 &= R^2+r^2+2R\rho,\\
C &= \frac{1}{\pi}\cdot\mu_0\cdot N\cdot i,
\end{aligned}$$

where μ_0 is the permeability of free space. The functions $K(m)$ and $E(m)$ are the complete elliptic integrals of the 1st and 2nd kinds respectively, defined [8] as

$$K(m) = \int_0^{\frac{\pi}{2}} \frac{1}{\sqrt{1-m\sin^2(w)}}dw,$$

$$E(m) = \int_0^{\frac{\pi}{2}} \sqrt{1-m\sin^2(w)}\;dw.$$

The magnetic field produced by the entire 3-D Helmholtz coil system can be expressed as the sum of the fields produced by the individual coils. This is because air is a linear medium and the superposition principle holds. While (3), (4), and (5) describe the flux density produced by a loop in the axial z direction, the field generated by coils positioned along the x and y axes can be easily found by swapping the spatial variables x,y,z. Noting from (3), (4), (5) that the flux density is a linear function of the loop current, the field $\mathbf{b}(x,y,z)$ due to all six windings is a linear combination of the six driving currents and it can be expressed as

$$\mathbf{b}(x,y,z) = \mathbf{A}(x,y,z)\cdot\mathbf{i}, \tag{6}$$

where $\mathbf{i}$ is the current vector

$$\mathbf{i} = \begin{bmatrix} i_{XF} & i_{XB} & i_{YL} & i_{YR} & i_{ZT} & i_{ZB}\end{bmatrix}^T.$$

The matrix $\mathbf{A}$ is a function of the point of interest $P(x,y,z)$ and of the geometrical properties of the coils as dictated by the field equations (3), (4), and (5). Each column of $\mathbf{A}$ represents the magnetic field when the current of the respective coil is unity and all other coils are turned off. Eq. (6) allows to map the coil driving currents to the magnetic flux density at any point in free space.

When dimensioning a coil design, a simpler expression for the field along the axial direction can be useful. Setting $x=y=0$, it is $b_x=b_y=0$ due to symmetry and (5) becomes

$$b_z = \frac{1}{2}\mu_0 Ni\cdot\frac{R^2}{[R^2+(z-d)^2]^{3/2}}.$$

Authorized licensed use limited to: Princeton University. Downloaded on November 14,2026 at 21:21:41 UTC from IEEE Xplore. Restrictions apply.

TABLE I
COIL-SYSTEM CHARACTERISTICS

Wdg*	N	R [cm]	d [cm]	$R_{cu}^{\dagger}$ [mΩ]	L [mH]	$L_s^{\ddagger}$ [mH]
X_o	56	15.2	9.7	154.4	1.71	6.70
X_i	64	16.5	7.2	188.3	2.38	
Y_o	48	12.2	8.5	107.1	0.94	3.78
Y_i	54	13.5	6.3	133.5	1.35	
Z_o	40	10.0	6.6	74.8	0.50	1.78
Z_i	40	11.1	4.8	79.5	0.54	

*subscripts o and i for the outer and inner windings respectively
†at room temperature 25°C
‡measured series inductance reflecting magnetic coupling

The flux density due to a pair of identical coils carrying current i is thus

$$b_z = \frac{\mu_0 N i R^2}{2} \cdot \left[\frac{1}{[R^2 + (z-d)^2]^{3/2}} + \frac{1}{[R^2 + (z+d)^2]^{3/2}} \right], \tag{7}$$

and the field at the origin is

$$b_z = \frac{\mu_0 N i R^2}{(R^2 + d^2)^{3/2}}. \tag{8}$$

Each loop of the coil system of Fig. 1 is made of 10 AWG square copper magnet wire and it is composed of 2 individual windings, an inner one and an outer one that are connected in series. The characteristics of the system are summarized in Table I.

Applying the field equations (3), (4), (5) for the specific coil system yields the following matrix **A** in [mT/A] at the origin:

$$\mathbf{A}(0,0,0) = \begin{bmatrix} 0.326 & 0.326 & 0 & 0 & 0 & 0 \\ 0 & 0 & 0.322 & 0.322 & 0 & 0 \\ 0 & 0 & 0 & 0 & 0.322 & 0.322 \end{bmatrix}. \tag{9}$$

The maximum possible flux density is practically limited by the ohmic resistance of the windings. While the field scales linearly with the driving current, the heat dissipation has a quadratic dependence. Fig. 3 shows the calculated magnetic field at the origin as a function of the coil input-power requirement at 25°C when both coils of each coaxial pair are driven with the same current.

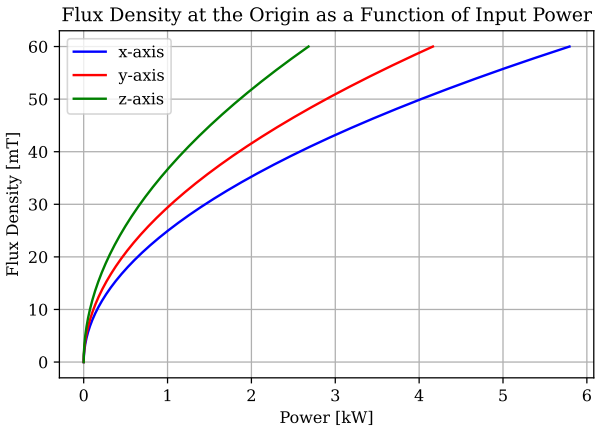


Fig. 3. Flux density at origin for the x, y, and z axis coil pairs as a function of the coil input power. Higher radius coils require more power to produce the same magnetic field.

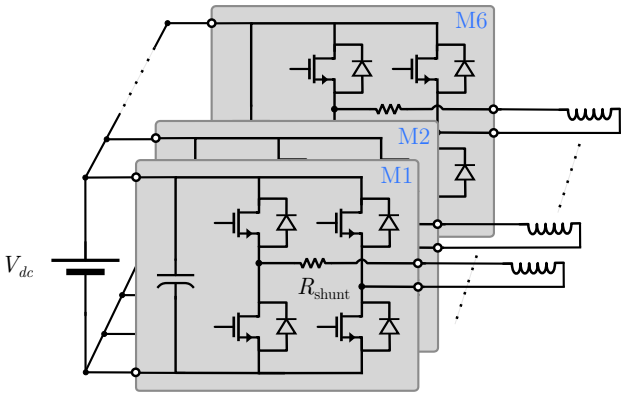


Fig. 4. Modular power-converter topology consisting of six full-bridge submodules to precisely control the current of each winding. The winding currents are sensed locally at each submodule using shunt resistors. A closed loop current-control scheme regulates the currents to the desired values.

B. Drive System

The inherent current-filtering nature of the coils allows the windings to be energized by a pulsed voltage source. A modular dc-ac converter topology is implemented, as shown in Fig. 4, to precisely control the currents of the individual windings. The coils are driven independently by six full-bridge submodules operating from a common dc bus.

The implemented power converter, shown in Fig. 1, employs 100 V top-cooled Si power MOSFETs switching at 10 kHz. It can operate at a maximum input voltage of 80 V, supplying a current up to 100 A per submodule for robotic control. The main components of the drive system are presented in Table II. To reduce the conduction loss which is dominant at this switching frequency, each switch is implemented by connecting two power MOSFETs in parallel. A copper heat sink is mounted on the top side of each submodule and two fans provide forced convection cooling for the entire six-unit stack, as shown in Fig. 5. A single-input half-bridge gate driver with programmable dead time and a bootstrap supply circuit is used for simplicity and minimal PWM signal count requirement from the control hardware. An input dc-bus capacitance of 6.2 mF is evenly distributed among the submodules by using surface mount solid polymer aluminum capacitors. To reduce the harmonic content of the magnetic field, a unipolar PWM switching scheme [9] was implemented resulting in an effective output switching frequency of 20 kHz.

To ensure a predictable transient response and to keep the coil currents stable at the desired setpoint irrespective of the temperature conditions affecting the resistance of the copper windings, a proportional-integral current-control scheme is

Authorized licensed use limited to: Princeton University. Downloaded on November 14,2026 at 21:21:41 UTC from IEEE Xplore. Restrictions apply.

TABLE II
POWER CONVERTER COMPONENTS

Component	Description
Power Switch	Infineon IPTC014N10NM5, 100 V
Gate Driver	TI LM5106 with bootstrap supply
DC-link Capacitor	Kemet A767MU226M2A, 22 μF, 100 V
Shunt Resistor	Bourns CSS2H-5930K-1L00FE, 1 mΩ
Current Sense Amplifier	TI INA241A2IDDFR
Control Hardware	TMS320F2837 control card

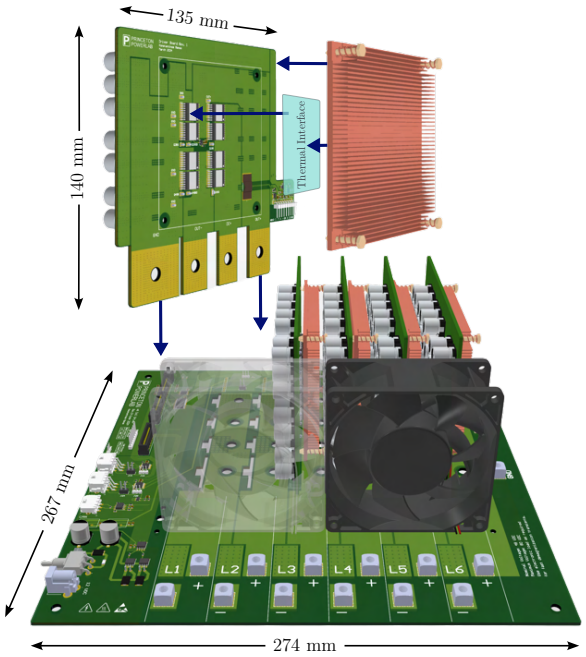


Fig. 5. The proposed modular drive is scalable allowing the use of an arbitrary number of full-bridge submodules to meet the coil-system requirements.

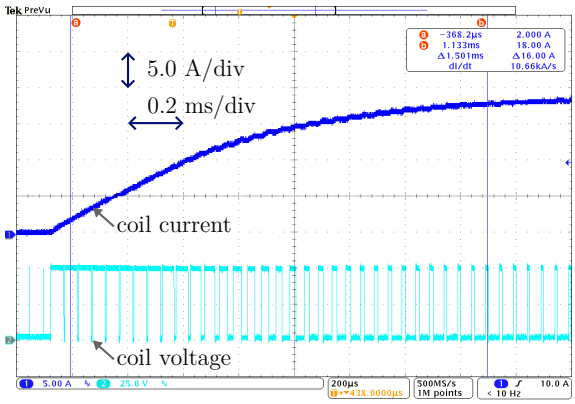


Fig. 6. Current step response from 0 to 20 A (blue) and pulse-width-modulated voltage (cyan) for $t_r = 1.5$ ms and $V_{dc} = 48$ V.

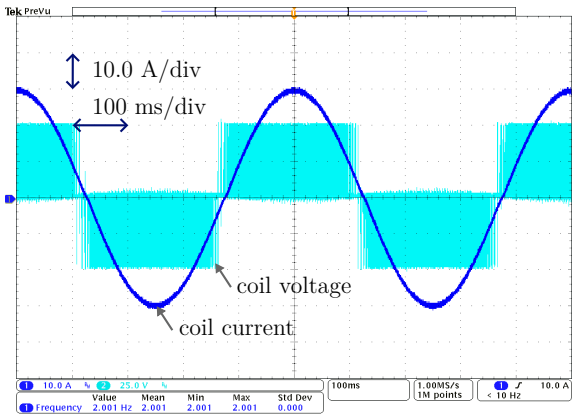


Fig. 7. Winding current (blue) and pulse-width-modulated voltage (cyan) for the Helmholtz coils. The system is capable of modulating an arbitrary signal from dc to 25 Hz with a maximum di/dt of 10 A/ms.

implemented. Selecting the controller gains as

$$k_p = \frac{L_s}{t_r} \ln 9, \tag{10}$$

$$k_i = \frac{R_s}{t_r} \ln 9, \tag{11}$$

results in a first order reference-to-output system with a rise time t_r. The rise time corresponds to the time it takes for the current to go from 10% to 90% of its final value. In the expressions above, L_s and R_s are the equivalent series inductance and the resistance of each inner-outer coil pair, as provided in Table I.

III. EXPERIMENTAL RESULTS & APPLICATIONS

The current tracking performance of the drive is first verified by triggering a step response, as shown in Fig. 6, where a rise time of 1.5 ms was chosen. An arbitrary current waveform can subsequently be generated by providing a sequence of reference values to the controller, as illustrated in Fig. 7.

The wireless actuation capability of the system is demonstrated by precisely controlling the motion of simple cubic robot structure. A nickel-plated N52-grade neodymium permanent magnet is embedded at the center of a 3D-printed block, as shown in Fig. 8. The robot motion is monitored in real time by motion capture cameras (e-con Systems NileCAM25CUOAGX) mounted around the Helmholtz-coil structure. Fiducial markers [10] are attached on the sides of the cubic block and a script employing the OpenCV [11] library runs in real time on a Jetson AGX Orin computer to detect the robot position and orientation. The parameters of the robotic structure are summarized in Table III.

When the same-axis coils are energized with identical current values, an approximately uniform magnetic field is generated inside the coil system. By manipulating the direction and magnitude of the flux density, the torque exerted on the magnetized robot can be precisely controlled, resulting in a well defined motion. This is illustrated in Fig. 9, where by imposing appropriate current waveforms on the coils, the robot can move by rolling in any direction as the induced electromagnetic torque, given by (1), tends to align the dipole moment $\mathbf{m}$ with the externally imposed magnetic field $\mathbf{b}$.

Authorized licensed use limited to: Princeton University. Downloaded on November 14,2026 at 21:21:41 UTC from IEEE Xplore. Restrictions apply.

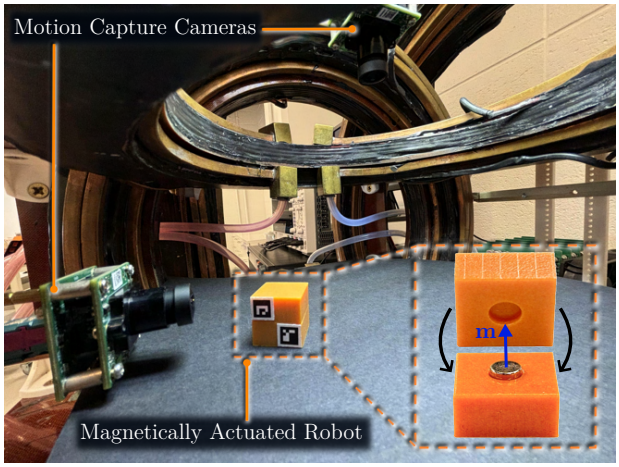


Fig. 8. Magnetically actuated robot inside the coil system. A neodymium permanent-magnet disc with an out-of-plane magnetization is placed inside a cubic-block structure.

TABLE III
ROBOTIC BLOCK PARAMETERS

Description	Value
Permanent magnet diameter	6.35 mm
Permanent magnet thickness	3.18 mm
Permanent magnet flux density	1.48 T
Cubic block material	UV-curable resins
Cubic block side length	20 mm
Assembled robot weight	10.3 g

IV. CONCLUSIONS

This paper discusses the modeling and design of a 3-D Helmholtz coil system for the wireless control of magnetically actuated robots. A modular dc-ac converter is designed to drive the 3-D Helmholtz coil resulting in a system capable of generating magnetic fields from dc to 25 Hz up to 60 mT in any direction. The developed hardware is employed to precisely control the motion of a magnetized cubic robot.

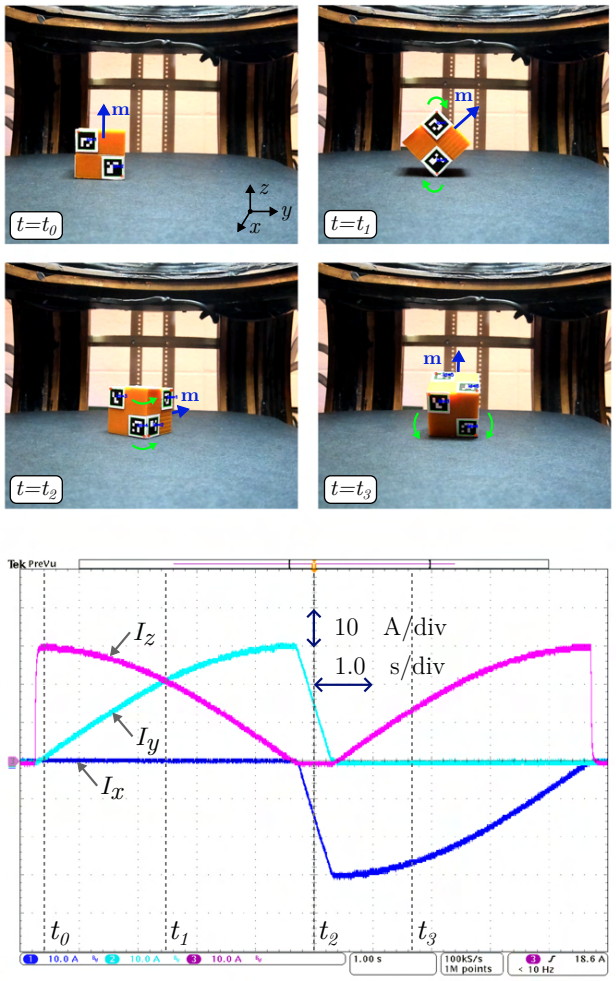


Fig. 9. The motion of the cube can be precisely controlled by generating an appropriate magnetic field. Initially, the robot rests on its face, with its magnetization $\mathbf{m}$ pointing upwards along the positive z direction. The externally imposed flux density $\mathbf{b}$ begins to rotate clockwise on the yz plane ($t = t_0$). The resulting electromagnetic torque causes the robot to move to the right by rolling clockwise around its edge ($t = t_1$). To change the direction of motion, the heading of the robot is adjusted by controlling the direction of $\mathbf{b}$ on the xy plane. As a result, the robot spins around its center of mass ($t = t_2$), allowing it to subsequently move along the x axis ($t = t_3$).

REFERENCES

[1] J. J. Abbott, E. Diller, and A. J. Petruska, "Magnetic methods in robotics," *Annual Review of Control, Robotics, and Autonomous Systems*, vol. 3, no. Volume 3, 2020, pp. 57–90, 2020.

[2] J. A. Levy, M. A. Straker, J. M. Stine, L. A. Beardslee, and R. Ghodssi, "Magnetically triggered ingestible capsule for localized microneedle drug delivery," *Device*, p. 100438, 2024.

[3] M. Sitti, *Mobile microrobotics*. Mit Press, 2017.

[4] S. Yim and M. Sitti, "Design and rolling locomotion of a magnetically actuated soft capsule endoscope," *IEEE Transactions on Robotics*, vol. 28, no. 1, pp. 183–194, 2012.

[5] Y. Kim, E. Genevriere, P. Harker, J. Choe, M. Balicki, R. W. Regenhardt, J. E. Vranic, A. A. Dmytriw, A. B. Patel, and X. Zhao, "Telerobotic neurovascular interventions with magnetic manipulation," *Science Robotics*, vol. 7, no. 65, p. eabg9907, 2022. [Online]. Available: https://www.science.org/doi/abs/10.1126/scirobotics.abg9907

[6] S. Wu, Q. Ze, J. Dai, N. Udipi, G. H. Paulino, and R. Zhao, "Stretchable origami robotic arm with omnidirectional bending and twisting," *Proceedings of the National Academy of Sciences*, vol. 118, no. 36, p. e2110023118, 2021. [Online]. Available: https://www.pnas.org/doi/abs/10.1073/pnas.2110023118

[7] J. C. Simpson, J. E. Lane, C. D. Immer, R. C. Youngquist, and T. Steinrock, "Simple analytic expressions for the magnetic field of a circular current loop," 2001.

[8] M. Abramowitz, *Handbook of Mathematical Functions, With Formulas, Graphs, and Mathematical Tables,*. USA: United States Department of Commerce, National Bureau of Standards, 1972.

[9] D. G. Holmes and T. A. Lipo, *Modulation of Single-Phase Voltage Source Inverters*. Wiley-IEEE Press, 2003, pp. 155–213. [Online]. Available: https://doi.org/10.1109/9780470546284.ch4

[10] S. Garrido-Jurado, R. Muñoz-Salinas, F. J. Madrid-Cuevas, and M. J. Marín-Jiménez, "Automatic generation and detection of highly reliable fiducial markers under occlusion," *Pattern Recognition*, vol. 47, no. 6, pp. 2280–2292, 2014. [Online]. Available: https://doi.org/10.1016/j.patcog.2014.01.005

[11] G. Bradski, "The OpenCV Library," *Dr. Dobb's Journal of Software Tools*, 2000.

Authorized licensed use limited to: Princeton University. Downloaded on November 14,2026 at 21:21:41 UTC from IEEE Xplore. Restrictions apply.